

Solvent Effects on the Self-Assembly of 1-Bromoeicosane on Graphite. Part I. Scanning Tunneling Microscopy

Gina M. Florio,^{*,†} Boaz Ilan,^{‡,§} Thomas Müller,^{‡,||} Thomas A. Baker,[‡] Adam Rothman,[‡] Tova L. Werblowsky,^{‡,⊥} B. J. Berne,[‡] and George W. Flynn^{*,‡}

Department of Chemistry and Department of Physics, St. John's University, Queens, New York 11439, and Department of Chemistry and Columbia Center for Electron Transport in Molecular Nanostructures, Columbia University, New York, New York 10027

Received: October 17, 2008; Revised Manuscript Received: December 17, 2008

Self-assembled monolayers of 1-bromoeicosane ($\text{BrC}_{20}\text{H}_{41}$) have been investigated at the vacuum–graphite and liquid–graphite interfaces using scanning tunneling microscopy (STM) (Part I) and theory (Part II). Under ultrahigh vacuum conditions at 80 K, STM images show 1-bromoeicosane in a lamellar assembly structure where individual molecules are predominantly arranged with their bromine groups pointed head-to-head with a $66 \pm 3^\circ$ angle between the lamella direction and the molecular backbone axis. A significant degree of disorder is observed under vacuum conditions, in which head-to-tail defects are interspersed throughout the film. When 1-bromoeicosane monolayers are formed and imaged in equilibrium with solution at ~ 290 K, the molecules again pack with their bromines oriented head-to-head but shift to form a nearly rectangular array. Subtle changes are observed depending on the solvent utilized, with the lamella–backbone angle varying between $81 \pm 3^\circ$ and $90 \pm 2^\circ$, and the corresponding intermolecular spacing ranging from 0.36 ± 0.02 to 0.46 ± 0.05 nm. The differences between the vacuum- and solution-based packing, as well as the possibility of two different packing structures occurring in solution, are discussed in light of the joint experimental and theoretical analysis.

Introduction

As technological advances require the fabrication of nanoscale structures, electronic devices, and sensors, a realistic design protocol relies on the self-assembly of small-scale components into larger, more sophisticated, functional architectures.^{1–4} Nature provides ubiquitous examples of self-assembled structures facilitated by the optimization of weak, noncovalent, intermolecular interactions such as dispersion forces and hydrogen bonding. The design of self-organizing systems provides a synthetic approach to the formation of nanomaterials whose structure and function are programmed by their chemistry.^{5,6}

Understanding molecular self-assembly offers insight into the programming of nano- and macroscale assembly.⁷ For molecules forming physisorbed monolayers on a surface but lacking covalent intermolecular interactions, a subtle balance of weak forces is responsible for directing the assembly. The formation of two-dimensional self-assembled networks of organic molecules on solid supports serves as an ideal model system in which to explore the additive nature of the weak forces giving rise to particular assembly patterns under a range of chemical and environmental conditions. When the assembly occurs in the presence of a solvent, the collective noncovalent interactions

must be energetically favorable with respect to the competing factors of solvent interaction and entropy.^{2,7}

While the majority of the STM studies of molecular self-assembly at the liquid–solid interface have focused on the elucidation of structural factors,^{8–11} several important investigations have probed the role of the solvent in defining the assembled structure. Observation of molecular exchange between the supernatant and the surface^{12–14} indicates that the solvent facilitates formation of a dynamic equilibrium between molecules in solution and those adsorbed in the monolayer. Changes in monolayer structure have been observed in air-based STM measurements for adsorbate molecules drop cast or spin-coated into films and subsequently interrogated in the absence of a solvent versus the same molecules deposited and imaged in equilibrium with a solution.^{15,16} There are examples of solvent inclusion in monolayers,^{17–24} particularly for those systems in which the solvent and solute contain hydrogen-bonding moieties. Solvent-induced polymorphism has been reported in which systematic variations in the solvent structure^{22,25,26} or polarity^{27,28} alter the packing structure formed by the adsorbate. Finally, solvent composition has been shown to influence the mobility and adsorption stability of molecules at interfaces^{13,29} as well as their chirality.²⁸

In the present work, a direct comparison is made between the assembly structures formed by 1-bromoeicosane ($\text{BrC}_{20}\text{H}_{41}$) molecules on graphite under ultrahigh vacuum (UHV) and solvent conditions using scanning tunneling microscopy (STM). This is part I of a joint experimental and theoretical report explicitly monitoring the role played by different solvents in the self-assembly of this simple halogenated alkane. Part II details the theoretical modeling of 1-bromoeicosane monolayers on graphite under vacuum, using implicit solvent and explicit solvent conditions via classical force field potential energy

* Corresponding authors. G. M. Florio. E-mail: floriog@stjohns.edu. Telephone: 718-990-2638. Fax: 718-990-1876. G. W. Flynn. E-mail: gwfl@columbia.edu. Telephone: 212-854-4162. Fax: 212-932-1289.

[†] St. John's University.

[‡] Columbia University.

[§] Current address. Schrödinger, L.L.C., New York, NY 10036.

^{||} Current address. Veeco Instruments, Inc., Santa Barbara, CA 93117.

[⊥] Current address. Department of Natural Sciences, Touro College, New York, NY 10010.

surface calculations and molecular dynamics simulations.³⁰ Direct comparison of the self-assembly morphologies under both solvent and vacuum conditions using experimental and theoretical methodologies provides unique insight into solvent effects on the assembly process.

Methods

I. UHV-STM. Ultrahigh vacuum STM experiments were conducted in a chamber with a base pressure of 1×10^{-10} Torr. The UHV chamber is equipped with a quadrupole mass spectrometer (Stanford Research Systems, RGA 200) and a variable-temperature STM (Omicron Vakuumphysik), along with other surface analysis instrumentation. Highly oriented pyrolytic graphite (HOPG) (Momentive Performance Materials, ZYB grade) was freshly cleaved and immediately introduced into the vacuum system. The HOPG was cleaned by annealing to ~ 980 K for 20 min and cooled to near room temperature prior to deposition of the molecular adsorbate.

Thin films of 1-bromoeicosane, BrC₂₀ (Aldrich, 98%), were prepared by vacuum sublimation in a small extension chamber attached to the main UHV chamber with a base pressure of $\sim 10^{-7}$ Torr. The evaporator consists of a resistively heated molybdenum crucible and a type-K thermocouple. The BrC₂₀ sample was degassed by heating to 310 K for 12–24 h prior to each deposition and was heated to 310–315 K for deposition onto the room-temperature, freshly annealed, and cleaved HOPG substrate. The deposition rate (8–10 Å/min) was monitored with a quartz crystal microbalance (Sigma Instruments). The sample was then transferred into the main UHV chamber and slowly annealed to 350–355 K. This gentle annealing process is intended to remove multilayers and give the remaining monolayer sufficient time and thermal energy to reach a minimum free energy structure. Because no information regarding thermal desorption of BrC₂₀ from graphite was found in the literature, deposition and annealing temperatures were estimated using the corresponding data for *n*-alkanes on graphite. Extrapolation of boiling point data as a function of chain length for a series of 1-bromoalkanes³¹ yields an approximate boiling point for BrC₂₀ of 665 K, which is identical to that of an *n*-alkane of similar mass (*n*-C₂₄H₅₀). The deposition and annealing temperatures were therefore estimated using the temperature-programmed desorption data for *n*-C₂₄H₅₀,³² in which rapid desorption of multilayers was observed at 315 K while monolayer desorption occurred at 440 K. Prior to the acquisition of STM images, the sample temperature was slowly lowered to 80 ± 5 K using a liquid helium flow cryostat with the tip constant at room temperature.

STM tips were prepared by electrochemical alternate current (ac) etching of polycrystalline tungsten wire. All images were taken in constant current mode. Typical scanning conditions are a +2 V bias between the tip and the surface, a 100 pA tunneling current, and a scan rate of 6–8 Hz. The effects of thermal and mechanical drift were minimized through use of the real-time drift correction available in the Omicron imaging software. Specific tunneling parameters are given for individual images in the figure captions, with the sign of the voltage referenced to the sample. A low-pass filter has been applied to the UHV-STM data, and care was taken not to distort the image during the filtering process.

II. Ambient STM. Complementary STM experiments were performed at the liquid–graphite interface between 17 and 20 °C. Topographic images were obtained using a NanoScope IIIa STM (Veeco Instruments, Inc.). Solutions of BrC₂₀ were prepared at or near saturation in a series of solvents: tetradecane,

1-phenyloctane, 1,2,4-trichlorobenzene, octanoic acid, 1-bromododecane, undecanol, and 1,2-dichlorobenzene. While no direct attempt was made to quantify the concentration of the solutions at saturation, BrC₂₀ is highly soluble in each solvent; the solubility of BrC₂₀ is in excess of 100 mg/mL in 1-phenyloctane at room temperature. Because no concentration dependence was observed on the molecular self-assembly of BrC₂₀ in 1-phenyloctane, it was not investigated for the other solvents. All chemicals were obtained commercially from Aldrich or Fluka ($\geq 95\%$ purity) and used without further purification. STM tips were mechanically cut Pt–Ir (87/13%) thermocouple wire (Omega Engineering, Inc.). For scanning in 1,2-dichlorobenzene, STM tips were insulated with a thin layer of Apiezon wax or polymer glue to reduce spurious solution current. To ensure accurate monolayer characterization by STM, the piezoelectric tube scanners were calibrated in *X* and *Y* prior to imaging in each solvent using graphite as a standard.³³ Postcalibration distance measurements between features on the graphite surface were within 3–5% of the known values. To form and image the monolayer, ~ 10 μ L of the desired solution was deposited onto the basal plane of freshly cleaved HOPG. Typical tunneling parameters for molecular imaging are -1.5 V, 300 pA, and a scan rate of 6–8 lines/s. Tunneling parameters are given for individual images in the captions, with the sign of the voltage referenced to the surface.

An extensive data set of 275 STM images was collected for BrC₂₀ at the liquid–solid interface to provide accurate measurements of monolayer parameters and to allow incorporation of the standard deviation as error bars on the measurements. The monolayer parameters discussed here are defined on the STM image in Figure 1d. The double lamella width (*a*), corresponding to the spacing across two molecules in adjacent lamellae, is reported as the average of 29 individual measurements for monolayers formed in all solvents. The angle between the molecular axis and the lamella direction (ϕ) reported here is the average value of a minimum of 32 individual measurements per solvent. The spacing between individual molecules (*b*) is measured along the lamella direction over 8–10 molecular spacings, providing an initial average value. Tabulated data are the average values of a minimum of 16 such measurements per solvent. The values reported in Tables 1 and 2 are the perpendicular intermolecular spacing ($b_{\perp} = b \sin \phi$) values, where the factor of $\sin \phi$ accounts for the offset due to angle ϕ between the lamella direction and the molecular axis. Care was taken to exclude images with poor resolution, large amounts of noise, or thermomechanical drift from the quantitative analysis. The error values reported are the standard deviations for each measurement. The percentage relative standard deviation (%RSD) for nearly every measurement mirrors the precision obtained for the bare graphite calibration. Analogous measurements were performed on vacuum data sets to obtain monolayer structural parameters.

Results

I. Structure of the Monolayer on Graphite: Vacuum versus Solvent. STM topographic images of 1-bromoeicosane (BrC₂₀) monolayers on the basal plane of graphite obtained under ultrahigh vacuum conditions are shown in panels a and b of Figure 1. The STM topographs depict the formation of lamellar arrays on graphite. The bromine endgroup appears as a bright protrusion in the images while the alkyl chain is less bright, as observed for other 1-haloalkanes under vacuum.^{34,35} The monolayer structure observed for BrC₂₀, while clearly more disordered, is nearly identical to that of 1-bromohexane (BrC₆)

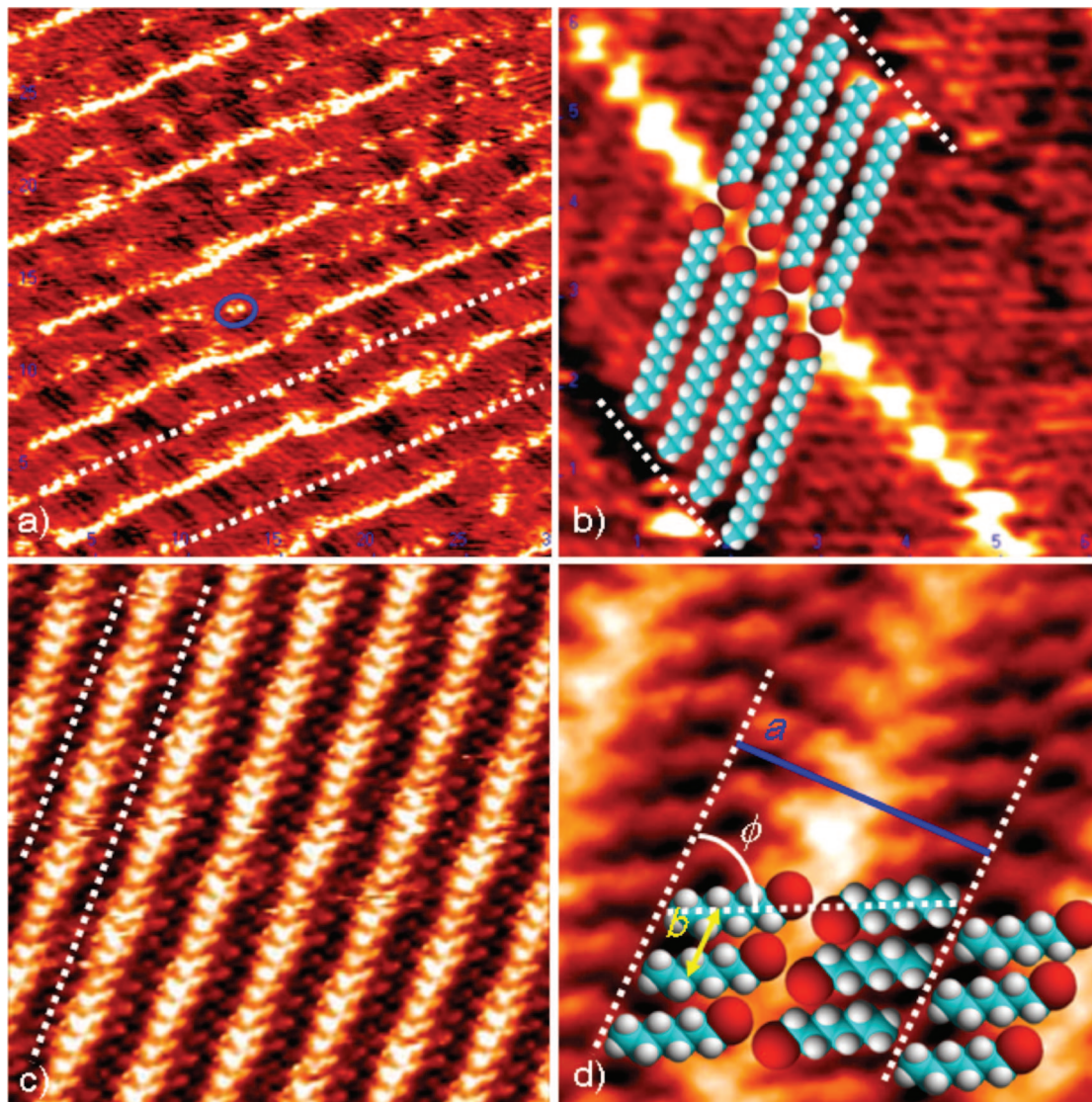


Figure 1. UHV-STM images of (a,b) 1-bromoeicosane and (c,d) 1-bromohexane monolayers on graphite at 80 K. (a) A 30 nm \times 30 nm image of 1-bromoeicosane recorded at +1.9 V, 80 pA, and 7 Hz and (b) a 6 nm \times 6 nm portion of (a) with a properly scaled molecular model. (c) A 14 nm \times 14 nm image of 1-bromohexane recorded at +2.0 V, 100 pA, and 7 Hz and (d) a 4 nm \times 4 nm portion of (c) with a properly scaled molecular model. Structural parameters (a , b , and ϕ) are defined in (d). The double lamella width is indicated in (a–d) by dashed white lines. The blue circle in (a) identifies a defect in the packing structure.

TABLE 1: Structural Parameters Measured from UHV-STM Images of the 1-Bromoalkane Monolayers at the Vacuum–Graphite Interface at 80 K

molecule	double lamella width (a) ^a	double lamella width (a) ^b (%RSD)	intermolecular distance (b_{\perp}) ^c	intermolecular distance (b_{\perp}) ^b (%RSD)	lamella–backbone angle (ϕ) ^d	lamella–backbone angle (ϕ) ^b (%RSD)
1-bromohexane	1.73 \pm 0.02	1.16	0.44 \pm 0.03	6.82	57 \pm 3	5.26
1-bromoeicosane	5.12 \pm 0.02	0.39	0.44 ^e	N/A	66 \pm 3	4.55

^a The double lamella width (nm) is the spacing between the dashed white lines in the STM images (Figure 1a), corresponding to two 1-bromoalkane molecules associated in a head-to-head arrangement. ^b The percentage relative standard deviation (%RSD) is the mean value of the corresponding measurement. ^c The perpendicular intermolecular distance (nm) corresponding to $b_{\perp} = b \sin \phi$ (Figure 1). ^d The lamella–backbone angle (deg) corresponding to the parameter labeled ϕ in Figure 1. ^e Estimated from the BrC₆ UHV-STM and from the BrC₂₀ calculations (Part II).³⁰

(Figure 1c,d)³⁴ in which the molecules form a bromine head-to-head assembly pattern with a 66 \pm 3° angle between the lamella direction and molecular axis (labeled ϕ in Figure 1). Structural parameters measured from the UHV-STM images of both molecules are reported in Table 1. The spacing between two rows of BrC₂₀ molecules is 5.12 \pm 0.02 nm, as indicated by the dashed white lines in Figure 1a. This double lamella width is approximately twice the length of a single molecule (2.60 nm) and is consistent with adsorption in an extended, all-

trans configuration. Because of the significant degree of disorder in the BrC₂₀ monolayer film, the intermolecular distance between alkyl chains within a given lamella is difficult to quantify. Theoretical analysis of the BrC₂₀ monolayers gives an intermolecular spacing of \sim 0.44 nm for molecules lying flat on the graphite surface.³⁰ This is in excellent agreement with the intermolecular distance measured from UHV-STM images of BrC₆ of \sim 0.44 nm.³⁴ Molecular models showing the packing structures of BrC₂₀ and BrC₆ are overlaid on the high-resolution

TABLE 2: Structural Parameters Measured from STM Images of 1-Bromoeicosane (BrC₂₀) Monolayers at the Liquid–Graphite Interface at 290–293 K^a

solvent	lamella–backbone angle (ϕ) ^b	lamella–backbone angle (ϕ) ^c (%RSD)	intermolecular distance (b_{\perp}) ^d	intermolecular distance (b_{\perp}) ^e (%RSD)	dielectric constant ^e
vacuum	66 ± 3	4.55	0.44 ^f	N/A	1.00
tetradecane	81 ± 2	2.47	0.38 ± 0.02	5.26	2.03
1-phenyloctane	83 ± 2	2.41	0.38 ± 0.02	5.26	2.26
1,2,4-trichlorobenzene	86 ± 2	2.33	0.36 ± 0.02	5.56	2.24
octanoic acid	87 ± 2	2.30	0.42 ± 0.02	4.76	2.85
1-bromododecane	88 ± 1	1.14	0.44 ± 0.02	4.55	4.07
undecanol	88 ± 2	2.27	0.46 ± 0.05	10.9	5.98
1,2-dichlorobenzene	89 ± 1	1.12	0.44 ± 0.09	20.5	9.93

^a UHV-STM data are given for comparison. ^b The lamella–backbone angle (deg) corresponding to the parameter labeled ϕ in Figures 1 and 2. Error values are the standard deviations for the measurements. ^c The percentage relative standard deviation (%RSD) is the mean value of the corresponding measurement. ^d The perpendicular intermolecular distance (nm) corresponding to $b_{\perp} = b \sin \phi$ (Figures 1 and 2). ^e The dielectric constant of each solvent (relative to vacuum) as reported in the *CRC Handbook of Chemistry and Physics*, 84th ed., 2003–2004. ^f Estimated from the BrC₆ UHV-STM and from the BrC₂₀ calculations (Part II).³⁰

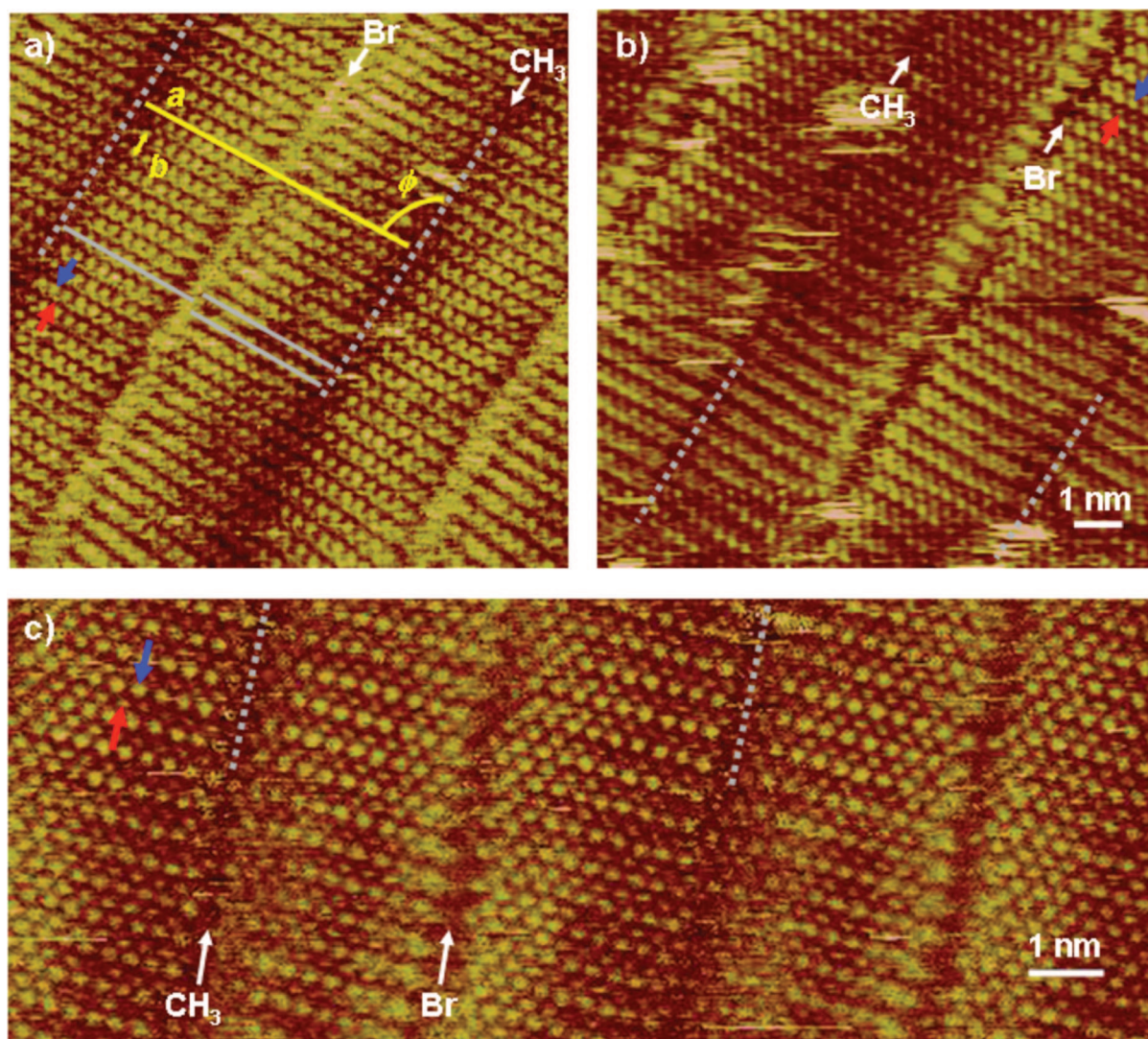


Figure 2. STM topographic images of 1-bromoeicosane at the liquid–graphite interface. (a) A 10 nm × 10 nm image of 1-bromoeicosane in 1,2,4-trichlorobenzene recorded at –1.50 V, 300 pA, and 8.72 Hz. (b) A 10 nm × 10 nm image of 1-bromoeicosane in tetradecane recorded at –1.40 V, 150 pA, and 15.3 Hz. (c) A 15 nm × ~6 nm image of 1-bromoeicosane in octanoic acid recorded at –1.50 V, 250 pA, and 7.629 Hz. Structural parameters (a , b , and ϕ) are defined in (a) and in Figure 1d. The dashed lines in (a–c) indicate the double lamella width. The solid gray lines in (a) indicate the position of individual molecules. The blue and red arrows in (a–c) indicate the bright and less bright hydrogen atoms of methylene units along the alkyl chain, respectively. The white arrows in (c) indicate the orientation of the molecules by pointing out the methyl–methyl and bromine–bromine interactions between molecules of neighboring lamellae. Images (a) and (b) have been low-pass filtered.

UHV-STM images in panels b and d of Figure 1, respectively. These models are consistent with the global minima on the potential energy surface of each system as determined via

theoretical modeling.^{30,34} The alignment of the molecules with respect to the underlying graphite lattice is determined by switching the tunneling conditions during a scan from a large

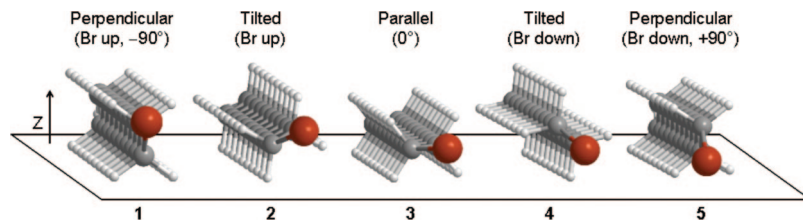


Figure 3. Edge-on view of possible orientations of 1-bromoeicosane relative to the surface plane. The molecules are shown in the extended, all-trans conformation with the terminal bromine vector behaving as an extension of the alkyl chain. Bromine atoms are indicated in red, carbon atoms in gray, and hydrogen atoms in white. A full 180° rotation of the molecule relative to the surface converts the orientation from 1 to 5.

gap resistance to a small gap resistance (Supporting Information). The molecules are found to align along a major axis of the graphite lattice, which is favorable according to theoretical calculations presented in Part II.³⁰

The BrC₂₀ monolayers formed and imaged under vacuum show a substantial degree of disorder and a large number of packing defects. Head-to-tail defects are observed in all imaged areas of the monolayers, an example of which is indicated by the blue oval in Figure 1a. This is in stark contrast to the monolayers formed under vacuum by BrC₆ (Figure 1c), for which virtually no packing defects are observed in any of the areas imaged. A major difference between BrC₆ and BrC₂₀ is the ratio of headgroup to total chain length. The smaller ratio for BrC₂₀ suggests that differences in energy between head-to-tail and head-to-head configurations would be small on a per chain basis. The combined effect of the larger surface adhesion energy, which increases the diffusion barrier, and the presence of a vacuum above the surface prevent mismatched BrC₂₀ molecules from readily desorbing to allow properly oriented (thermodynamically most stable) molecules to take their place in the monolayer. Images obtained for the BrC₂₀ monolayer at ~245 K still show the same degree of disorder (data not shown). The thermal energy afforded the system by the gentle annealing process following deposition and/or imaging near room temperature appears to be insufficient for complete ordering of the BrC₂₀ monolayers.

Representative STM topographic images of the monolayers formed by BrC₂₀ at the liquid–graphite interface are shown in Figure 2, and the corresponding structural data are summarized in Table 2. At the liquid–solid interface, the molecules form head-to-head morphologies characterized by lamella–backbone angles (ϕ) between $81 \pm 3^\circ$ and $90 \pm 2^\circ$, in contrast to the $\sim 60^\circ$ lamella–backbone angle observed under UHV conditions (Figure 1a,b). The intermolecular distances (b_\perp) for films at the liquid–graphite interface vary between 0.36 ± 0.02 and 0.46 ± 0.05 nm. For solvents in which monolayers form with a lamella–backbone angle less than 90° , a compressed intermolecular spacing of ~ 0.38 nm is observed (Table 2). This occurs despite the fact that the intermolecular spacing for monolayers commensurate with the graphite lattice is 0.426 nm (for a molecular backbone extended parallel to the graphite surface), whether they have a 90° or 60° lamella–backbone angle. The double lamella width (dashed gray lines in Figure 2) is measured to be $a = 5.39 \pm 0.30$ nm, just over twice the length of a single molecule (2.60 nm), which is again consistent with molecules being adsorbed in an extended, all-trans configuration. Within the double lamella, the two rows of molecules are offset relative to each other (solid gray lines in Figure 2a).

In contrast to vacuum conditions, STM topographic imaging of BrC₂₀ under solvent conditions predominantly shows the bromine atoms as regions of low tunneling probability (dark). Previous STM studies of bromine-functionalized alkane derivatives at the liquid–graphite and –MoS₂ interfaces have shown

that bromine functional groups sometimes appear dark,^{36–38} sometimes appear bright,^{8,37,39–42} and sometimes switch between the two states.^{39–42} In the present work, the bromine endgroup was occasionally observed to switch between low and high contrast over large regions of the monolayer film. This switching was observed exclusively under solvent conditions.

The potential origins of the switching phenomenon have been discussed at length in the literature,^{8,37–43} several of which will be highlighted briefly here. First, a trans-to-gauche conformational change in the bromine endgroup of a molecular adsorbate has been suggested to occur with the gauche orientation pointing the bromine toward the STM tip, thereby enhancing its image contrast.^{39,40,43,44} The energy barrier to conformational isomerization is unknown for the adsorbate in vacuum; furthermore, how this barrier will change in the presence of a solvent or for a concerted trans–gauche isomerization of a large swath of molecules is also not obvious. The solvent is expected, however, to lower the energy of this structural change (compared to a vacuum) given its ability to solvate the bromine atom. The trans–gauche isomerization argument does not explain the observation of bright bromine functionalities in nonterminal positions along an alkyl chain.⁸ Alternatively, molecules at the liquid–solid interface could undergo orientation changes by tilting or rolling, involving the rotation of the molecular backbone relative to the plane of the substrate (Figure 3 and discussion below).⁴⁵ In principle, this would cause the bromine atoms to point up toward the STM tip at times and down toward the graphite at other times. Finally, while tip effects cannot be ruled out with certainty, the fact that the bromine endgroups are always observed as bright under vacuum conditions on graphite between 80 and 245 K suggests an explanation involving the presence of a solvent as the key modifying factor. It is possible that the change in image contrast is due to an electronic effect modifying the tunneling probability associated with the presence of a solvent as compared to a vacuum in the tunnel junction. In any scenario, it is clear that the solvent facilitates a structural and/or electronic change that is not observed under vacuum conditions.

II. Monolayer Structure as a Function of a Solvent. To further explore the role a solvent plays in the self-assembly of BrC₂₀, STM images of monolayers derived from a series of solvents were obtained. The solvents were chosen on the basis of the variation of their structure, polarity, and interaction with the solute. In addition, they are designed to fulfill the deposition criteria of high solubility and low vapor pressure. The solvents included *n*-alkanes and their derivatives (tetradecane, 1-phenyloctane, 1-bromododecane, 1-undecanol, and octanoic acid) as well as two aromatic solvents (1,2,4-trichlorobenzene and 1,2-dichlorobenzene). For all solvents, the BrC₂₀ molecules form highly ordered, lamellar monolayer structures, exhibiting very few, if any, packing defects.

Under solvent conditions monolayer films are formed with a nearly perpendicular orientation of the lamella with respect to

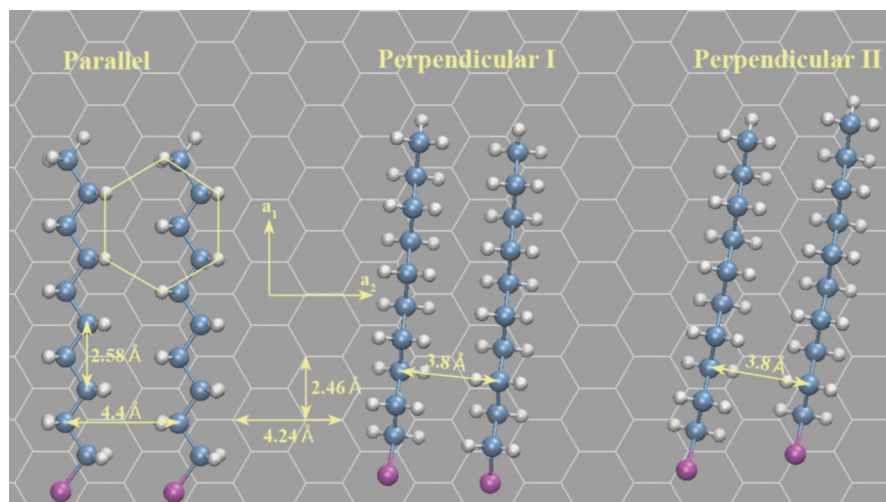


Figure 4. The calculated (using molecular dynamics simulations for energy-minimized structures) alignment of pairs of 1-bromodecane ($\text{BrC}_{10}\text{H}_{21}$) molecules on a model graphite surface with their chains in parallel (left) or perpendicular (center, right) arrangements relative to the surface. The two perpendicular structures give rise to (I) a near 90° and (II) an 80° lamella–backbone angle. Relevant structural information is included for the molecules and the graphite lattice.

the molecular backbone, in contrast to the 60° -angled structures observed under vacuum. However, subtle variations from the 90° lamella–backbone morphology are seen in the solution-based monolayer films (Table 2). The lamella–backbone angle ranges in value from approximately 80° in tetradecane to 90° in 1,2-dichlorobenzene. Concomitantly, the intermolecular spacing varies from about 0.38 nm for films with smaller lamella–backbone angles to more than 0.42 nm for films with 90° lamella–backbone angles (Table 2). The origin of these subtle structural differences is presently unknown but potentially indicates the formation of at least two distinct monolayer structures at the liquid–graphite interface. Because the relative standard deviations of the monolayer structural parameters are on the order of the error in the STM calibration,⁴⁶ the measurements of angles and intermolecular spacing appear to be different outside the limits set by experimental error, thereby supporting the existence of (on average) two different monolayer structures under solvent conditions.

Observation of films with an intermolecular distance of ~ 0.38 nm is notable because of the fact that the distance is shorter than the intermolecular distance for the energetically favored parallel alignment of the molecular backbone with respect to the graphite surface (0.44 nm)³⁰ as well as the corresponding lattice spacing of graphite (0.426 nm). In order to achieve such a tightly packed structure, it is possible that the molecules are not lying with their alkyl chains perfectly flat on the graphite surface. Configurations for which the molecular backbones are tilted to any extent with respect to the graphite surface are expected to show a compressed intermolecular spacing as compared to that of the surface parallel orientation of alkyl chains. Several representative orientations of a single BrC_{20} molecule on the graphite surface are shown in Figure 3. The entire molecule (alkyl backbone and bromine endgroup) is in the extended, all-trans configuration. From left to right, the molecule completes a 180° rotation relative to the surface plane (the rolling or tilting angle). Perpendicular configurations (**1**, **5**) are those in which the molecular backbone is rotated $\pm 90^\circ$ with respect to the surface such that the bromine is pointed either away from (up/–) or toward the surface (down/+). For the parallel configuration (**3**) the carbon backbone is completely parallel to the surface at a rolling angle of 0° . For all tilted configurations, those with rolling angles between 0° and $\pm 90^\circ$,

the carbon atoms of neighboring methylene units are at different heights above the surface (e.g., **2** and **4**). For the tilted and perpendicular structures, the fact that the carbon atoms of neighboring methylene units lie at different heights above the graphite surface gives rise to less favorable dispersion interactions with the graphite lattice as compared to that of the parallel configuration. However, it is possible that achieving a compressed intermolecular spacing in a tilted configuration would increase dispersion interactions between neighboring chains, thereby stabilizing an out-of-plane configuration.

The possibility that the apparent intermolecular compression is due to out-of-plane tilting of the molecular backbone has been further examined quantitatively according to energy minimizations of pairs of 1-bromodecane ($\text{BrC}_{10}\text{H}_{21}$) molecules oriented parallel and perpendicular to the surface plane (Figure 4). Two different perpendicular orientations are considered: one in which the molecules are oriented with their backbones and bromine endgroups down/up ($+90^\circ/-90^\circ$) and one in which the molecules are up/up ($-90^\circ/-90^\circ$). These formations were chosen as representative of the effects because of alternating and identical orientations of neighboring bromine atoms. The perpendicular formations were generally observed to be highly unstable under vacuum conditions, even at very low temperatures, whereas an explicit undecanol solvent calculation tends to stabilize the perpendicular configurations.³⁰ Tilted configurations between 0° and 90° were observed to reorient to either 90° or 0° , depending on whether the starting tilt angle was larger or smaller than 45° , respectively.³⁰ The minimized structure of a parallel set of chains (far left in Figure 4) gives rise to a lamella–backbone angle of 90° . Molecules adsorbed parallel to the graphite surface have an intermolecular spacing of ~ 0.44 nm, which is approximately commensurate with the underlying graphite along the a_2 principle lattice direction. The stability of this structure arises from the favorable adsorbate–substrate interaction and the interdigitation of the neighboring alkyl chains, which aligns the hydrogen atoms into a hexagonal arrangement nearly commensurate with the graphite lattice (sketched hexagon in Figure 4).

Perpendicularly oriented 1-bromoalkane molecules can be arranged in several possible ways, two of which (labeled I and II) have been examined for the model case of BrC_{10} (center and far right in Figure 4). The pair of neighboring molecules

in structure I adopt alternating -90° (up) and $+90^\circ$ (down) out-of-plane orientations. For this arrangement, the monolayer has a lamella–backbone angle of slightly less than 90° . In structure II, both molecules are in the -90° (up) out-of-plane configuration. For this arrangement, the monolayer depicts a lamella–backbone angle of $\sim 80^\circ$. For both perpendicular structures I and II, the intermolecular spacing is ~ 0.38 nm. The calculated intermolecular distance of ~ 0.38 nm and lamella–backbone angle of $\sim 80^\circ$ for the perpendicular configurations suggest that the monolayer structures observed in the experiments may consist of molecules aligned with their backbones perpendicular or at least strongly tilted with respect to the graphite surface. However, in contrast to theoretical predictions, the experiments depict a characteristic hexagonal signature hydrogen atom arrangement for the $\sim 80^\circ$ lamella–backbone formations, suggesting that the backbone skeletons do not deviate strongly from a parallel configuration. Note that the calculations were done for the vacuum interface case and do not take into account possible solvation of the bromine atom at the liquid–solid interface. The inclusion of a solvent, however, is not expected to modify significantly the calculated intermolecular distances for the perpendicular (~ 0.38 nm) and parallel (~ 0.44 nm) orientations of the backbone skeleton. A corresponding energy minimization performed on similar length *n*-alkanes also depicts an intermolecular distance of ~ 0.38 nm, whereas the lamella–backbone angle is exactly 90° .³⁰ This suggests that unfavorable interactions between bromine atoms from the nearest neighboring chains in the perpendicular out-of-plane alignment may be responsible for the deviations from the 90° lamella–backbone angle. Nevertheless, at least for the vacuum–solid interface case, the potential energy of the parallel configuration (left pair of chains in Figure 4) is lower by approximately 2.5 and 7 kcal mol⁻¹ molecule⁻¹ relative to the perpendicular configurations (I and II), respectively.⁴⁷ In a parallel configuration, each carbon atom, as well as the bromine headgroup, is at nearly the same distance above the graphite surface, thereby maximizing van der Waals and image charge interactions between the atoms and the surface, and thus minimizing the potential energy of adsorption. It is for this reason that low-lying conformational minima on the potential energy surfaces of 1-bromoalkanes on graphite have the molecules adsorbed completely flat, such that the entire backbone skeleton is parallel to the graphite surface (Figure 3, structure 3 and Figure 4, leftmost structure).^{30,35}

Given the experimental observation of two different assembly structures at the liquid–graphite interface, a natural question arises as to what role a solvent plays, if any, in dictating which structure is observed. To this end, the only apparent correlation we have found is an approximate relationship between the dielectric constant and the lamella–backbone angle such that lower dielectric constant solvents produce monolayers with smaller angles (Table 2). The trend is intriguing and may signal the importance of bromine solvation in modifying the identity of the lowest-energy self-assembled structures.

Discussion

Molecular self-assembly of 1-bromoeicosane at the graphite–solvent interface displays two morphologies characterized by $\sim 80^\circ$ and $\sim 90^\circ$ angles between the molecular axis and the lamella direction with corresponding intermolecular distances (b_\perp) of ~ 0.38 and 0.44 nm, respectively. On the other hand, the morphology observed under vacuum conditions is characterized by a $\sim 60^\circ$ lamella–backbone angle with b_\perp estimated to be 0.44 nm on the basis of the value measured from UHV-STM images of BrC₆,³⁴ as well as the theoretical analysis of

BrC₂₀.³⁰ The molecules align with their bromine atoms head-to-head under both vacuum and solvent conditions. The structure of the self-assembled monolayer formed by 1-bromoeicosane on graphite under ultrahigh vacuum conditions is generally consistent with that found for the series of 1-haloalkanes,³⁴ except that long chain species exhibit more disorder in their shorter counterpart films. The solvent-based 90° lamella–backbone structure is similar to that observed previously for 1-bromodocosane (BrC₂₂H₄₅) and other haloalkanes under analogous solvent conditions.^{8,36,39,40} The measured intermolecular distance of ~ 0.44 nm matches closely that expected for BrC₂₀, having its backbone aligned parallel with respect to the graphite surface. Theoretical calculations carried out for chains lying parallel to the graphite surface confirm that the 90° lamella–backbone morphology is unstable under vacuum conditions and undergoes a transition to a 60° lamella–backbone structure. The presence of an explicit solvent in the modeling stabilizes the 90° lamella–backbone morphology, in agreement with the experiment.

The observation of a second morphology under solvent conditions characterized by an intermolecular distance of ~ 0.38 nm and a lamella–backbone angle of $\sim 80^\circ$ is, however, surprising because the close-packed condition for chains lying parallel to the graphite surface in the extended all-trans configuration is achieved by a well-defined, discrete series of lamella–backbone angles (90° , 60° , 40.89° , 30° , etc.).³⁰ This suggests that the second solvent-based monolayer structure could be formed by chains lying with their molecular backbone either perpendicular or tilted with respect to the graphite surface. The theoretical analysis supports such a configuration to the extent that the calculated intermolecular distance for perpendicularly oriented chains (0.38 nm) is in agreement with that measured for the $\sim 80^\circ$ lamella–backbone structure. At the same time, in the presence of an explicit undecanol solvent layer, tilted configurations with out-of-plane angles of less than 90° were observed to be unstable. This discrepancy casts some doubt on the possibility of tilted configurations, although it must be remembered that the theoretical computations involving a solvent for these types of self-assembled systems are in their infancy.

While it is difficult to rule out the tilted configurations with certainty, the observations of a compressed intermolecular spacing and less than 90° lamella–backbone angle in some solvents could also be accounted for by the coexistence of an equal number of parallel- and perpendicular-oriented molecules, as has been suggested by a neutron scattering study of a dotriacontane (*n*-C₃₂D₆₆) monolayer covered by a partial second layer of hexane on graphite.⁴⁸ Two pieces of evidence from the STM images argue against such a structural model for the samples investigated in the present study. First, the spot patterns observed in high-resolution STM topographs of the monolayers formed from solvent (e.g., Figure 2b) suggest that all of the molecules are oriented in an identical fashion along the lamella direction, thus ruling out an alternating perpendicular–parallel structure within a given lamella as suggested by Herwig et al.⁴⁸ This leaves the possibility of domains consisting of all parallel-oriented and all perpendicular-oriented molecules. In the STM images of BrC₂₀ under all solvents, multiple domains were infrequently observed. For images where multiple domains are detected, the molecules were observed to have identical packing structures and differ only in their orientation with respect to the lattice vectors of the graphite. Moreover, the $\sim 80^\circ$ lamellae–backbone morphologies depict a hexagonal arrangement of the top hydrogen atoms, suggesting that the backbones lie at least approximately parallel to the graphite surface

(sketched hexagon in Figure 4). Of course, there exists the possibility that the molecules are fluxional on the (relatively slow) STM time scale, alternatively taking parallel or perpendicular orientations to the graphite surface.⁴⁵ Depending on the rate of exchange, which could easily be solvent dependent, compared to that of the typical STM image capture time scale of several seconds, molecules could appear in some average orientation that is not the most stable 90° form, thereby leading to apparent decreases in the measured intermolecular distance and the lamella–backbone angle. It is worth noting that solvent-driven stabilization or destabilization of molecules in the liquid phase above the interface can be expected to affect the rate of interchange between the solution and the surface, even if a solvent does not directly lower the energy of the adsorbed species.

Both the scenario corresponding to the coexistence of parallel and perpendicular orientations, and the possibility of fluctuations in the tilting angle offer an explanation for the alternating image contrast of the bromine atoms. It is not entirely clear why some solvents favor monolayer morphologies with a compressed intermolecular spacing and a less than 90° lamella–backbone angle. The upward-tilted, downward-tilted, and parallel orientations of the bromine headgroup are expected to exhibit varied electrostatic (multipole) interactions with the atoms of the graphite or solvent, possibly explaining the stability of one structure over the other.

A lateral compression of the intermolecular spacing in the adsorbate monolayer upon increasing coverage has been observed by low-energy electron diffraction studies of multilayer formation in *n*-alkanes on graphite under vacuum.^{49,50} Molecular dynamics simulations bear out the experimental results for the *n*-alkanes,⁵¹ as well as a similar lateral compression phenomenon in rare gas films on graphite;⁵² however, the driving force for uniaxial compression in these simulations is attributed to a shift from incommensurate to commensurate film formation. These results suggest that a monolayer film structure can be altered by changing the composition of the upper interface layer from a vacuum to a molecular or atomic substance. On the other hand, in the systems studied here, compression of the intermolecular spacing in the monolayer film observed under certain solvents seemingly results in a shift away from commensurability with the graphite lattice.

Careful analysis of high-resolution STM images at the liquid–graphite interface (Figure 2) reveals an intriguing asymmetric spot pattern for each molecule within all lamellae. The molecules display alternating bright (blue arrows) and dark (red arrows) rows of hydrogen atoms. While this asymmetric spot pattern would be consistent with, in principle, the tilted out-of-plane scenario (Figure 4), the pattern is observed for the 80° and 90° lamella–backbone morphologies with $b_{\perp} \sim 0.38$ and 0.44 nm, respectively. For the 90° lamella–backbone morphology, the chains are definitively oriented parallel to the graphite surface. In addition, the calculations depict the tilted configurations to be unstable.³⁰ An alternate explanation for the variation in this asymmetric spot pattern has been given by recent density functional theory (DFT) studies in our group.⁵³ These computations suggest that for chains oriented parallel to the graphite surface, the asymmetric spot pattern has an electronic structure origin.⁵³ It is well-known that the non-equivalent carbon atoms of the graphite lattice give rise to a local density of states at the surface that is localized on every other carbon atom.⁵⁴ The spot pattern observed in STM images of the bare graphite surface under typical tunneling conditions is itself reflective of this phenomenon.^{10,55} We have found that

the intensity modulation observed in STM images of alkanes, both in this work and in numerous literature examples,^{39,56–58} is reflective of the underlying graphite electronic structure due to coupling of the molecular frontier orbitals to the nonequivalent carbons of type *A* and *B* of the substrate associated with the *ABAB* stacking of the graphite lattice.

Conclusions

The molecular self-assembly of 1-bromoeicosane on graphite has been investigated using a combined STM and theoretical approach. STM measurements reveal differences in the structure, image contrast, and degree of order of the monolayers formed under ultrahigh vacuum versus solvent-based conditions. In addition, at the solvent–graphite interface, two monolayer assembly structures are observed, differing slightly in their lamella–backbone angle and interchain distances. Theoretical analyses of the system under vacuum and under model solvent conditions support most of the experimental findings and provide a framework for understanding the structural preferences. A detailed analysis of the theoretical study and its findings can be found in the companion paper (Part II).³⁰ By direct comparison of the monolayer formation of 1-bromoeicosane on graphite under vacuum and solvent conditions, the presence of a solvent is shown unequivocally to influence the packing of a very simple molecule. In addition, STM imaging under ultrahigh vacuum conditions indicates that observed variations in image contrast of the bromine functionality are due to the presence of solvent. Moreover, subtle changes in the packing structure as a function of a solvent suggest that solvation plays an important and direct role in molecular self-assembly.

Acknowledgment. This work was funded by National Science Foundation (NSF) Grants CHE-07-01483 (to G.W.F.) and CHE-06-13401 (to B.J.B.). Partial support was provided by Nanoscale Science and Engineering Initiative of the National Science Foundation Award CHE-06-41523 and the New York State Office of Technology, Science, and Academic Research (NYSTAR). G.M.F. acknowledges funding from the Clare Boothe Luce Program of the Henry Luce Foundation (2005–present), the Camille and Henry Dreyfus Foundation’s Faculty Start-Up Award (2005), and the Camille and Henry Dreyfus Foundation’s Postdoctoral Program in Environmental Chemistry (2001). A.R. and T.A.B. were supported through the 2003 NSF–Research Experiences for Undergraduates (REU) programs of Columbia University’s Materials Research Science and Engineering Center (MRSEC) and Chemistry Department, respectively.

Supporting Information Available: A STM image of 1-bromoeicosane on graphite in vacuum showing directly the alignment of the alkane chain with the graphite lattice. This material is available free of charge via the Internet at <http://pubs.acs.org>.

References and Notes

- (1) Whitesides, G. M.; Grzybowski, B. Self-Assembly at All Scales. *Science* **2002**, 295 (5564), 2418–2421.
- (2) Whitesides, G. M.; Mathias, J. P.; Seto, C. T. Molecular Self-Assembly and Nanochemistry: A Chemical Strategy for the Synthesis of Nanostructures. *Science* **1991**, 254 (5036), 1312–1319.
- (3) Fitzgerald, M. Trying to Put New Zip Into Moore’s Law. *The New York Times*, Feb. 24, 2008.
- (4) Service, R. F. How Far Can We Push Chemical Self-Assembly. *Science* **2005**, 309 (5731), 95.
- (5) Lehn, J.-M. Supramolecular Chemistry and Self-Assembly Special Feature: Toward Complex Matter: Supramolecular Chemistry and Self-Organization. *Proc. Natl. Acad. Sci. U.S.A.* **2002**, 99 (8), 4763–4768.

- (6) Nguyen, S. T. G.; Gin, D. L.; Hupp, J. T.; Zhang, X. Supramolecular Chemistry: Functional Structures on the Mesoscale. *Proc. Natl. Acad. Sci. U.S.A.* **2001**, *98*, 11849–11850.
- (7) Whitesides, G. M.; Boncheva, M. Supramolecular Chemistry and Self-Assembly Special Feature: Beyond Molecules: Self-Assembly of Mesoscopic and Macroscopic Components. *Proc. Natl. Acad. Sci. U.S.A.* **2002**, *99* (8), 4769–4774.
- (8) Claypool, C. L.; Faglioni, F.; Goddard, W. A.; Gray, H. B.; Lewis, N. S.; Marcus, R. A. Source of Image Contrast in STM Images of Functionalized Alkanes on Graphite: A Systematic Functional Group Approach. *J. Phys. Chem. B* **1997**, *101* (31), 5978–5995.
- (9) De Feyter, S.; De Schryver, F. C. Self-Assembly at the Liquid/Solid Interface: STM Reveals. *J. Phys. Chem. B* **2005**, *109* (10), 4290–4302.
- (10) Giancarlo, L. C.; Flynn, G. W. Scanning Tunneling and Atomic Force Microscopy Probes of Self-Assembled, Physisorbed Monolayers: Peeking at the Peaks. *Annu. Rev. Phys. Chem.* **1998**, *49*, 297–336.
- (11) Plass, K. E.; Grzesiak, A. L.; Matzger, A. J. Molecular Packing and Symmetry of Two-Dimensional Crystals. *Acc. Chem. Res.* **2007**, *40* (4), 287–293.
- (12) Padowitz, D. F.; Messmore, B. W. STM Observations of Exchange Dynamics at the Solid-Liquid Interface Using a Molecular Tracer. *J. Phys. Chem. B* **2000**, *104* (43), 9943–9946.
- (13) Schull, G.; Douillard, L.; Fiorini-Debuisschert, C.; Charra, F.; Mathevet, F.; Kreher, D.; Attias, A. J. Single-Molecule Dynamics in a Self-Assembled 2D Molecular Sieve. *Nano Lett.* **2006**, *6* (7), 1360–1363.
- (14) Takajo, D.; Nemoto, T.; Kurata, H.; Isoda, S.; Ozaki, H.; Mazaki, Y. Replacement of Molecules at Liquid/Solid Interfaces. *Thin Solid Films* **2003**, *438–439*, 428–432.
- (15) Shao, X.; Luo, X. C.; Hu, X. Q.; Wu, K. Chain-Length Effects on Molecular Conformation in and Chirality of Self-Assembled Monolayers of Alkoxyated Benzo[c]cinnoline Derivatives on Highly Oriented Pyrolytic Graphite. *J. Phys. Chem. B* **2006**, *110* (31), 15393–15402.
- (16) Yang, X.; Mu, Z.; Wang, Z.; Zhang, X.; Wang, J.; Wang, Y. STM Study on Quinacridone Derivative Assemblies: Modulation of the Two-Dimensional Structure by Coadsorption with Dicarboxylic Acids. *Langmuir* **2005**, *21*, 7225–7229.
- (17) Nath, K. G.; Ivashenko, O.; MacLeod, J. M.; Miwa, J. A.; Wuest, J. D.; Nanci, A.; Perepichka, D. F.; Rosei, F. Crystal Engineering in Two Dimensions: An Approach to Molecular Nanopatterning. *J. Phys. Chem. C* **2007**, *111* (45), 16996–17007.
- (18) Nath, K. G.; Ivashenko, O.; Miwa, J. A.; Dang, H.; Wuest, J. D.; Nanci, A.; Perepichka, D. F.; Rosei, F. Rational Modulation of the Periodicity in Linear Hydrogen-Bonded Assemblies of Trimesic Acid on Surfaces. *J. Am. Chem. Soc.* **2006**, *128* (13), 4212–4213.
- (19) Tao, F.; Bernasek, S. L. Understanding Odd-Even Effects in Organic Self-Assembled Monolayers. *Chem. Rev.* **2007**, *107* (5), 1408–1453.
- (20) Qian, P.; Nanjo, H.; Yokoyama, T.; Suzuki, T. M.; Akasaka, K.; Orhui, H. Chiral Molecular Patterns of Self-Assembled Ion Pairs Composed of (*R,S*), (*S*)-16-Methyloctadecanoic Acid and 4,4-Bipyridine. *Chem. Commun.* **2000**, *20*, 2021–2022.
- (21) De Feyter, S.; Gesquiere, A.; Abdel-Mottaleb, M. M.; Grim, P. C. M.; De Schryver, F. C.; Meiners, C.; Sieffert, M.; Valiyaveetil, S.; Mullen, K. Scanning Tunneling Microscopy: A Unique Tool in the Study of Chirality, Dynamics, and Reactivity in Physisorbed Organic Monolayers. *Acc. Chem. Res.* **2000**, *33* (8), 520–531.
- (22) Kampschulte, L.; Griessl, S.; Heckl, W. M.; Lackinger, M. Mediated Coadsorption at the Liquid-Solid Interface: Stabilization through Hydrogen Bonds. *J. Phys. Chem. B* **2005**, *109*, 14074–14078.
- (23) Wintgens, D.; Yablon, D. G.; Flynn, G. W. Packing of HO(CH₂)(14)COOH and HO(CH₂)(15)COOH on Graphite at the Liquid-Solid Interface Observed by Scanning Tunneling Microscopy: Methylene Unit Direction of Self-Assembly Structures. *J. Phys. Chem. B* **2003**, *107* (1), 173–179.
- (24) Eichhorst-Gerner, K.; Stabel, A.; Moessner, G.; Declercq, D.; Valiyaveetil, S.; Enkelmann, V.; Mullen, K.; Rabe, J. P. Self-Assembly of a Two-Component Hydrogen-Bonded Network: Comparison of the Two-Dimensional Structure Observed by Scanning Tunneling Microscopy and the Three-Dimensional Crystal Lattice. *Angew. Chem., Int. Ed. Engl.* **1996**, *35* (13–14), 1492–1495.
- (25) Kampschulte, L.; Lackinger, M.; Mair, A.-K.; Kishore, R. S. K.; Griessl, S.; Schmittel, M.; Heckl, W. M. Solvent Induced Polymorphism in Supramolecular 1,3,5-Benzenetribenzoic Acid Monolayers. *J. Phys. Chem. B* **2006**, *110* (22), 10829–10836.
- (26) Lackinger, M.; Griessl, S.; Heckl, W. A.; Hietschold, M.; Flynn, G. W. Self-Assembly of Trimesic Acid at the Liquid-Solid Interface—A Study of Solvent-Induced Polymorphism. *Langmuir* **2005**, *21* (11), 4984–4988.
- (27) Klymchenko, A. S.; Schuurmans, N.; van der Auweraer, M.; Feringa, B. L.; van Esch, J.; De Feyter, S. Scanning Tunneling Microscopy of a Foldamer Prototype at the Liquid/Solid Interface: Water/Au(111) Versus 1-Octanol/Graphite. *New J. Chem.* **2006**, *30*, 1420–1428.
- (28) Li, C. J.; Zeng, Q. D.; Wang, C.; Wan, L. J.; Xu, S. L.; Wang, C. R.; Bai, C. L. Solvent Effects on the Chirality in Two-Dimensional Molecular Assemblies. *J. Phys. Chem. B* **2003**, *107* (3), 747–750.
- (29) Venkataraman, B.; Breen, J. J.; Flynn, G. W. Scanning-Tunneling-Microscopy Studies of Solvent Effects on the Adsorption and Mobility of Triacontane Triacontanol Molecules Adsorbed on Graphite. *J. Phys. Chem.* **1995**, *99* (17), 6608–6619.
- (30) Ilan, B.; Florio, G. M.; Müller, T.; Werblowsky, T. L.; Hybertsen, M. S.; Berne, B. J.; Flynn, G. W. Solvent Effects in the Self-Assembly of 1-Bromoeicosane on Graphite. Part II: Theory. *J. Phys. Chem. C* **2009**, *113* (9), 3641–3649.
- (31) Brown, R. L.; Stein, S. E. Boiling Point Data. <http://webbook.nist.gov>.
- (32) Paserba, K. R.; Gellman, A. J. Kinetics and Energetics of Oligomer Desorption from Surfaces. *Phys. Rev. Lett.* **2001**, *86* (19), 4338–4341.
- (33) *MultiMode SPM Instruction Manual*, Revision B; Veeco Instruments, Inc.: New York, 2004.
- (34) Müller, T.; Werblowsky, T. L.; Florio, G. M.; Berne, B. J.; Flynn, G. W. Ultra-High Vacuum Scanning Tunneling Microscopy and Theoretical Studies of 1-Halohexane Monolayers on Graphite. *Proc. Natl. Acad. Sci. U.S.A.* **2005**, *102* (15), 5315–5322.
- (35) Florio, G. M.; Werblowsky, T. L.; Ilan, B.; Müller, T.; Berne, B. J.; Flynn, G. W. Chain-Length Effects on the Self-Assembly of Short 1-Bromoalkane and *n*-Alkane Monolayers on Graphite. *J. Phys. Chem. C* **2008**, *112* (46), 18067–18075.
- (36) Claypool, C. L.; Faglioni, F.; Matzger, A. J.; Goddard, W. A.; Lewis, N. S. Effects of Molecular Geometry on the STM Image Contrast of Methyl- and Bromo-Substituted Alkanes and Alkanols on Graphite. *J. Phys. Chem. B* **1999**, *103* (44), 9690–9699.
- (37) Fang, H. B.; Giancarlo, L. C.; Flynn, G. W. Packing of Br(CH₂)(10)COOH and Br(CH₂)(11)COOH on Graphite: An Odd-Even Length Effect Observed by Scanning Tunneling Microscopy. *J. Phys. Chem. B* **1998**, *102* (38), 7421–7424.
- (38) Giancarlo, L. C.; Fang, H.; Rubin, S. H.; Bront, A. A.; Flynn, G. W. Influence of the Substrate on Order and Image Contrast for Physisorbed, Self-Assembled Molecular Monolayers: STM Studies of Functionalized Hydrocarbons on Graphite and MoS₂. *J. Phys. Chem. B* **1998**, *102* (50), 10255–10263.
- (39) Cyr, D. M.; Venkataraman, B.; Flynn, G. W. STM Investigations of Organic Molecules Physisorbed at the Liquid-Solid Interface. *Chem. Mater.* **1996**, *8* (8), 1600–1615.
- (40) Cyr, D. M.; Venkataraman, B.; Flynn, G. W.; Black, A.; Whitesides, G. M. Functional Group Identification in Scanning Tunneling Microscopy of Molecular Adsorbates. *J. Phys. Chem.* **1996**, *100* (32), 13747–13759.
- (41) Giancarlo, L. C.; Cyr, D. M.; Muyskens, K.; Flynn, G. W. Scanning Tunneling Microscopy of Molecular Adsorbates at the Liquid-Solid Interface: Functional Group Variations in Image Contrast. *Langmuir* **1998**, *14*, 1465–1471.
- (42) Chen, Q.; Yan, H.-J.; Yan, C.-J.; Pan, G.-B.; Wan, L.-J.; Wen, G.-Y.; Zhang, D.-Q. STM Investigation of the Dependence of Alkane and Alkane (C18H38, C19H40) Derivatives Self-Assembly on Molecular Chemical Structure on HOPG Surface. *Surf. Sci.* **2008**, *602* (6), 1256–1266.
- (43) Faglioni, F.; Claypool, C. L.; Lewis, N. S.; Goddard, W. A., III. Theoretical Description of the STM Images of Alkanes and Substituted Alkanes Adsorbed on Graphite. *J. Phys. Chem. B* **1997**, *101* (31), 5996–6020.
- (44) Crystal, J.; Zhang, L. Y.; Friesner, R. A.; Flynn, G. W. Computational Modeling for Scanning Tunneling Microscopy of Physisorbed Molecules via Ab Initio Quantum Chemistry. *J. Phys. Chem. A* **2002**, *106* (9), 1802–1814.
- (45) Liang, W.; Whangbo, M. H.; Wawkuszewski, A.; Cantow, H.-J.; Magonov, S. N. Electronic Origin of Scanning Tunneling Microscopy Images and Carbon Skeleton Orientations of Normal Alkanes Adsorbed on Graphite. *Adv. Mater.* **1993**, *5* (11), 817–821.
- (46) The one notable exception is the intermolecular spacing measured for films formed from 1,2-dichlorobenzene, in which the standard deviation itself is large because of the small number of images obtained for 1-bromoeicosane in this solvent as compared to that of the others. The high relative dielectric constant of 1,2-dichlorobenzene necessitating an insulated STM tip, coupled with its high relative vapor pressure, made imaging challenging.
- (47) The Steele contribution of the parallel configuration has been corrected by a factor of 0.38–0.44 to account for its larger packing area relative to the perpendicular configurations.
- (48) Herwig, K. W.; Matthies, B.; Taub, H. Solvent Effects on the Monolayer Structure of Long *n*-Alkane Molecules Adsorbed on Graphite. *Phys. Rev. Lett.* **1995**, *75* (17), 3154–3157.
- (49) Krim, J.; Suzanne, J.; Shechter, H.; Wang, R.; Taub, H. A LEED and Neutron Diffraction Study of Hexane Adsorbed on Graphite in the Monolayer Range: Uniaxial Commensurate Incommensurate Transition. *Surf. Sci.* **1985**, *162*, 446–451.
- (50) Arnold, T.; Thomas, R. K.; Castro, M. A.; Clarke, S. M.; Messe, L.; Inaba, A. The Crystalline Structures of the Even Alkanes Hexane,

Octane, Decane, Dodecane and Tetradecane Monolayers Adsorbed on Graphite at Submonolayer Coverages and From the Liquid. *Phys. Chem. Chem. Phys.* **2002**, *4* (2), 345–351.

(51) Krishnan, M.; Balasubramanian, S.; Clarke, S. An Atomistic Simulation Study of a Solid Monolayer and Trilayer of *n*-hexane on Graphite. *J. Chem. Phys.* **2003**, *118* (11), 5082–5086.

(52) Khandkar, M. D.; Balasubramanian, S. Argon Multilayers on a Corrugated Surface: Effect of Coverage on Structure. *Chem. Phys. Lett.* **2002**, *362* (1–2), 144–150.

(53) Ilan, B.; Florio, G. M.; Hybertsen, M. S.; Berne, B. J.; Flynn, G. W. Scanning Tunneling Microscopy Images of Alkane Derivatives on Graphite: Role of Electronic Effects. *Nano Lett.* **2008**, *8* (10), 3160–3165.

(54) Tomanek, D.; Louie, S. G. First-principles Calculation of Highly Asymmetric Structure in Scanning-Tunneling-Microscopy Images of Graphite. *Phys. Rev. B* **1988**, *37*, 8327–8336.

(55) Tomanek, D.; Louie, S. G.; Mamin, H. J.; Abraham, D. W.; Thomson, R. E.; Ganz, E.; Clarke, J. Theory and Observation of Highly Asymmetric Atomic Structure in Scanning-Tunneling-Microscopy Images of Graphite. *Phys. Rev. B* **1987**, *35*, 7790–7793.

(56) McGonigal, G. C.; Bernhardt, R. H.; Thomson, D. J. Imaging Alkane Layers at the Liquid Graphite Interface with the Scanning Tunneling Microscope. *Appl. Phys. Lett.* **1990**, *57* (1), 28–30.

(57) Rabe, J. P.; Buchholz, S. Commensurability and Mobility in 2-Dimensional Molecular-Patterns on Graphite. *Science* **1991**, *253* (5018), 424–427.

(58) De Feyter, S.; De Schryver, F. C. Two-Dimensional Supramolecular Self-Assembly Probed by Scanning Tunneling Microscopy. *Chem. Soc. Rev.* **2003**, *32* (3), 139–150.

JP809216W